IEEE Access
Multidisciplinary | Rapid Review | Open Access Journal

Received November 12, 2020, accepted December 9, 2020, date of publication December 15, 2020,
date of current version December 29, 2020.

Digital Object Identifier 10.1109/ACCESS.2020.3045006

Distance Estimation of High-Speed Underwater Targets Based on a Frequency-Coded Continuous Wave

GEUN-HO PARK[1], YOUNG-KWANG SEO[1], WAN-JIN KIM[2], AND HYOUNG-NAM KIM[1], (Member, IEEE)

[1]Department of Electronics Engineering, Pusan National University, Busan 46241, Republic of Korea
[2]Agency for Defense Development, Changwon 51499, Republic of Korea

Corresponding author: Hyoung-Nam Kim (hnkim@pusan.ac.kr)

This work was supported by the Institute of Information and Communications Technology Planning and Evaluation (IITP) Grant funded by the Korean Government (MSIT) (Information Protection Core Source Technology Development) under Grant 2019-0-00706.

ABSTRACT Robust and continuous distance estimation of a rapidly approaching threat is a significant concern in underwater technology. Although frequency modulated continuous waves (FMCWs) have been widely used in near-range situations, FMCWs are challenging to use in a specific underwater situation. If a high-speed underwater target appears, the target echo can no longer be modeled as a simple Doppler-shifted version of the wave, which increases the distance estimation error of conventional FMCW methods. This situation also requires frequent updates of distance estimates. Thus, to obtain the distance of a high-speed underwater target, we propose a signal format of a frequency coded continuous wave (FCCW) and develop an FCCW-based distance estimation scheme. The proposed distance estimation algorithm has three steps: group correlators and accumulated sum (GCAS), time-delay map (TDM), and Doppler line fitting (DLF). The structure of the proposed FCCW enables the detection of each frequency hopping time (FHT) within a shorter period than the observation time. The GCAS algorithm detects FHTs in the FCCW and is designed to easily extend the matched filter length, resulting in an extension of the acquisition time. The TDM and DLF provide robust distance estimates and enable the classification of multiple targets. Simulation results show that the proposed method can detect FHTs and estimate the target distance more stably in low signal-to-noise-ratio environments by increasing the matched filter's acquisition time.

INDEX TERMS Frequency coded continuous wave, Costas code, near-range sonar, high-speed target.

I. INTRODUCTION

SONAR (sound navigation and ranging) has been widely used to detect and identify various underwater targets [1]–[3]. An active sonar system, a well-known sonar technique, emits an acoustic wave and receives a target's echo. The reflected sound wave provides information on underwater targets such as target location, velocity, trajectory, and identification features.

The most common acoustic waveforms are a pulse signal and a continuous wave (CW) [4]–[6]. Conventional pulsed active sonars have duty cycles on the order of one percent, which indicates that 99% of the time is spent waiting for the reflected wave. Conversely, high duty cycle sonars such as continuous active sonars (CASs) have duty cycles approaching 100%.

The associate editor coordinating the review of this manuscript and approving it for publication was Jenny Mahoney.

CASs are beneficial for tracking moving targets because CASs provide near continuous updates, high precision, broadband reception, a high signal-to-noise ratio (SNR), and the capability to detect multiple targets [4]–[9]. These characteristics are based on the CW's signal structure, particularly in the difference of the duty cycle between a CW and a pulsed waveform.

Because unmanned underwater vehicles, which are fast and small, are increasingly widely used [10]–[12], CASs have garnered considerable attention. We also consider tracking faster and smaller underwater targets. Thus, this study primarily investigates CW waveforms.

A. RELATED WORK

A frequency modulated continuous wave (FMCW) is a representative technique that is used in short-range applications such as proximity fuses, level measurements, and collision

avoidance scenarios [13]–[17]. Early CASs used long slow linear frequency modulation (LFM), which is similar to the long-range version of the FMCW. However, only a small segment of a received wave is used in detection, where stretch processing is typically introduced; thus, the full waveform bandwidth is not used [18]. DeFerrari and Wylie proposed the use of M-sequence coded pulses as CAS transmission waveforms [19]. These waveforms achieve high-range resolution even when only a small segment with full bandwidth is coherently detected by repeatedly sweeping through the available hop frequencies and relying on varying the frequency sequences to prevent interference and range ambiguities [17]. Hickman and Krolik described a similar idea using Costas sequences identified as the slow-time-Costas-coded (SLO-CO) processing algorithm [20]. The primary features of these frequency coded continuous waves (FCCWs) are near-continuous updates, low transmission power, and suppression of range-Doppler ambiguities, which allow an active sonar to achieve a low probability of intercept (LPI). The short-time Fourier transform (STFT) can be considered [22] but cannot provide a flexible selection of signal length; thus, it is difficult to directly compare the proposed method and STFT.

B. MOTIVATION BEHIND THIS STUDY

This study focuses on a special FCCW for LPI underwater seekers. The FMCW has been widely used for radar seekers. The beat-frequency-based distance estimation processing for FMCW can estimate the distance of a target when the time-frequency slopes of the transmitted and received frequency modulations (FMs) are the same. However, beat-frequency-based distance-estimation processing cannot be applied to high-speed underwater sonar applications where time-frequency slope mismatches and pulse-length mismatches exist due to significant Doppler effect [21]–[23]. The presence of significant Doppler effect motivates us to develop a new method. However, for this reason, we also exclude FMCW for LPI underwater seekers due to its mismatch problems.

To use FCCW for an LPI underwater seeker, however, two things must be complemented. First, the method used should be applicable to situations where large Doppler effects exist and cause shrinkage or expansion of signal length and bandwidth in the range of 5–10% or more. Then, the target distance can be estimated even when the sonar and target have a relative speed of 40–80 knots. Second, in the estimation process, the acquisition time of the received wave must be extended to stably estimate target distance and velocity under low SNR environments. In LPI seeker systems, the power of a transmitter should be low and progressively reduce when approaching a target to evade early detection by an enemy radar or sonar [24].

C. CONSIDERATIONS OF THE STUDY

To update the distance estimate with a shorter period in a low SNR environment, we propose using group correlators and

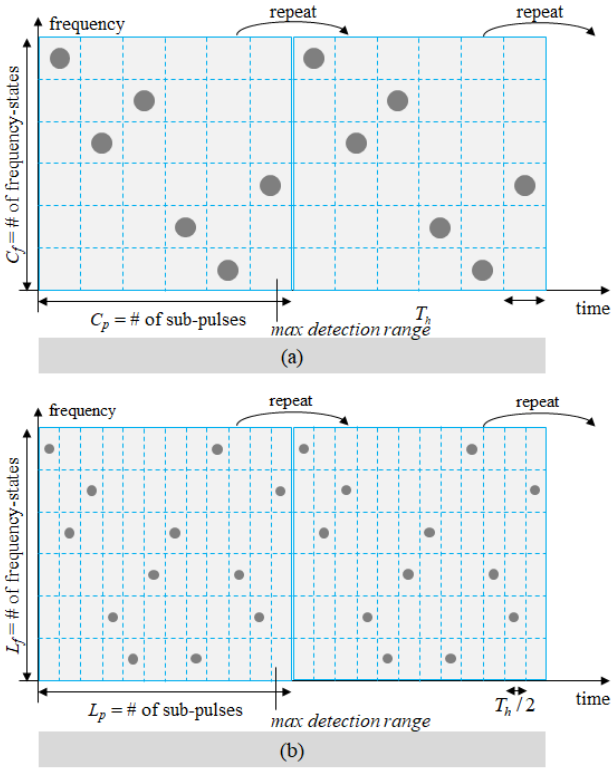

FIGURE 1. Time-frequency code array; (a) Costas array of order 6, (b) an example of the proposed time-frequency code array of order $L_f = 6$, $L_p = 12$.

an accumulated sum (GCAS) similar to the SLO-CO [20]. We can summarize the considerations for the design of FCCW and GCAS as follows:

1) To update the distance estimate with a shorter period, distances should be continuously estimated. In general, frequency coding allows us to control the side-lobe of the ambiguity function to suppress interference or reverberations. The Costas code is widely applied to frequency coded waveforms. The Costas array, which represents the time-frequency component of the transmitted wave, has the same number of frequency states and subpulses, as shown in Fig. 1-(a). However, to update the information estimate more often, the total number of subpulses must be larger than the number of frequency states, as shown in Fig. 1-(b). Distance estimates are obtained once every hopping interval (i.e., the length of a subpulse), and the sequential estimates plotted on a time-delay map directly represent an approaching threat.

2) To stably operate in high-speed underwater environments, the proposed distance estimation scheme uses matched filters (MFs) to detect each frequency hopping time (FHT) in the received FCCW. The MFs can manage shrinkage or expansion of signal length and bandwidth caused by the Doppler effect. The SLO-CO uses multiple MFs to detect all FHTs but does not consider the exact Doppler effect [20].

3) To reliably estimate distance in low SNR environments, the proposed distance estimation algorithm is suitable for

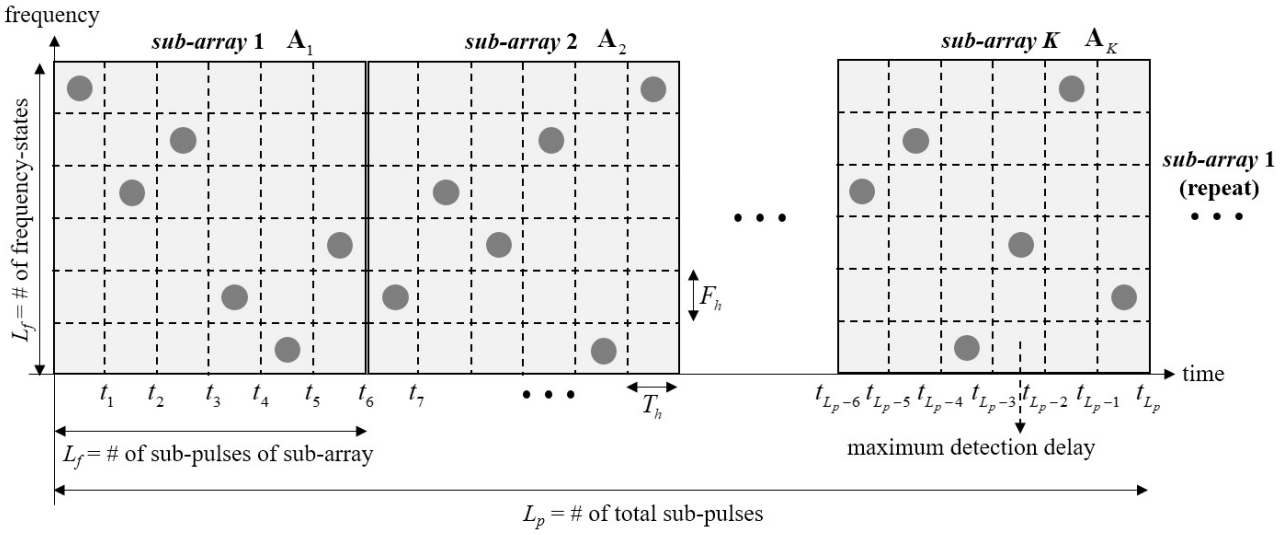

FIGURE 2. Example of time-frequency code array of the proposed frequency coded continuous wave.

filtering a continuous wave. The acquisition time can be extended as required to improve detection and estimation performance. We incorporate group correlators (GC) and accumulated sum (AS) to extend the MF's length with minimum computational increase. Increasing the MF lengths yields more reliable detection and estimation in low SNR environments. This property is useful for certain active sonar systems where anti-submarine or anti-torpedo sonars are required to work reliably in low SNR environments due to the LPI requirement.

D. CONTRIBUTIONS OF THE STUDY

The contribution of this paper can be summarized in the following two points:

1) The proposed signal design allows us to estimate the FHTs of a received FCCW using a time-frequency code array. We propose a time-frequency code array with more subpulses than frequency states to produce frequent updates of distance estimates.

2) We propose an efficient algorithm to update distance estimates more frequently. The proposed method also provides a way to select a flexible acquisition time, simplifying a desired increase in processing gain. This property is particularly effective in a low SNR environment. The estimation process of the proposed method has three steps: GCAS, time delay map (TDM), and Doppler line fitting (DLF).

E. OUTLINE

The remainder of this paper is organized as follows. In Section II, the details of the proposed FCCW are presented. The proposed distance estimation scheme is explained in Section III. In Section IV, the simulation results are presented, and conclusions are drawn in Section V.

II. FREQUENCY CODED CONTINUOUS WAVE (FCCW)

While frequency coding has been used to minimize or control the side-lobe level of an ambiguity function [25]–[27], we use it to obtain and distinguish multiple distance estimates within the maximum delay of the target reflected wave. The parameters related to FCCW generation in Fig. 1-(b) are summarized as follows:

- T_h: frequency hopping interval, length of the subpulse,
- F_h: hopping frequency,
- L_f: # of frequency states, # of subpulses of a subarray,
- L_p: # of total subpulses,
- K: # of subarrays,
- $\tau_{\max}$: maximum detection delay.

The time-frequency code array for the FCCW consists of K subarrays, as shown in Fig. 2. Each subarray consists of L_f subpulses with different center frequencies, which is similar to a Costas code array. The tone signal or LFM signal can be used as a subpulse. Once the available bandwidth and L_f are determined, K is set to satisfy the following condition:

$$T_h \cdot K \cdot L_f > \tau_{\max}. \tag{1}$$

Each subarray must have a different time-frequency code structure. Within a subarray, the subpulses must have different center frequencies. The related k^{th} subarray $\mathbf{A}_k$ and total time-frequency code array $\mathbf{A}$ are defined as follows:

$$\mathbf{A}_k \in \mathbb{R}^{L_f \times L_f}, \tag{2}$$

$$\mathbf{A} = [\mathbf{A}_1, \mathbf{A}_1, \cdots, \mathbf{A}_K] \in \mathbb{R}^{L_f \times L_p}, \tag{3}$$

where only one component of each column and each row of $\mathbf{A}_k$ is 1, and the other components are all 0, as shown in Fig. 2. L_f corresponds to the order of the Costas array, and various Costas arrays with the same order can also be used as the subarrays $\mathbf{A}_k$. The indices i and l of $\mathbf{A}$ (i, l) determine the

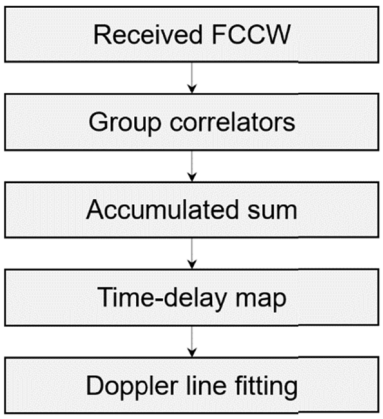

FIGURE 3. Distance estimation procedure for the FCCW.

carrier frequency and the shift-time of the subpulse, respectively. A generated wave with $\mathbf{A}$ is represented by

$$s(t) = \text{Real}\left\{\sum_{l}^{L_p}\sum_{i}^{L_f}\mathbf{A}(i,l)\,p(t-lT_h)e^{-j2\pi(f_c+(i-1)F_h)t}\right\}, \tag{4}$$

where f_c is the carrier frequency, f_h is the hopping frequency, and $p(t)$ is a baseband pulse of duration T_h and is a tone, LFM, or different types of pulses.

The purpose of the modified FCCW scheme is to stably determine the distance of a rapidly approaching target and to update it more frequently. To meet this frequent update requirement, we use a time-frequency code array $\mathbf{A}$ with more subpulses than frequency states. The primary purpose of frequency coding in $\mathbf{A}$ is not minimization of the side-lobe levels or the control of an ambiguity function but rather the classification of the FHTs of a received FCCW and the robust matching to their corresponding FHTs $\left[t_l,\ 1 \le l \le L_p\right]$ in the transmitted FCCW. However, to suppress the side-lobe of the ambiguity function, not more than two subpulses of the same center frequency can exist in the subarray.

III. DISTANCE ESTIMATION

As a target's distance is obtained by every FHT in the received FCCW signal, all FHTs should be robustly detected and classified. Fig. 3 shows the entire procedure of the proposed distance estimation scheme. Processing of the received signal consists of four steps: GC, AS, TDM, and DLF.

We also assume that the Doppler frequency of the target is known. The Doppler frequency of the target can be obtained from several Doppler correlators [29], and the proposed approach is easily implemented along with the Doppler correlators by simply expanding the proposed processing blocks.

To detect all FHTs, different MFs are required to detect the respective FHTs. The GC is implemented with MFs of adjustable lengths with unit correlators for each subpulse. In the AS process, the MF outputs of adjacent FHTs are accumulated to more stably perform FHT detection and distance estimation. The TDM is drawn by the AS outputs and is used for classification and distance estimation of multiple targets. In the DLF process, a curve-fitting algorithm is used to classify multiple targets that have the same Doppler frequency but different distances.

A. MATCHED FILTERING BASED ON GC

In this section, we introduce the GC-based implementation of MFs. The MFs are segments of the transmitted FCCW corresponding to each FHT, as shown in Fig. 4. There are variable-length MFs for detecting specific FHTs. The GC can implement all L_p MFs for detecting L_p FHTs using only L_f correlators corresponding to the subpulses.

The MF to detect FHT t_m is defined for $0 \le t \le L_m T_h/\kappa$ as follows:

$$h_m^{L_m}(t) = \sum_{l}^{L_m}\sum_{i}^{L_f}\mathbf{W}_m^{L_m}(i,l)\,p(t-T_h l)e^{-j2\pi\kappa(f_c+(i-1)F_h)t}, \tag{5}$$

where a GC's code array $\mathbf{W}_m^{L_m}$ is used to generate a specific MF $h_m^{L_m}(t)$ with L_m subpulses and corresponds to a specific section of the time-frequency code array $\mathbf{A}$, as shown in Fig. 4, and the Doppler ratio $\kappa = f_c^R/f_c^T$ is defined as the ratio of the transmitted center frequency f_c^T to the received center frequency f_c^R. An example of $\mathbf{W}_{10}^8$ shown in Fig. 4 is given by

$$\mathbf{W}_{10}^8 = \begin{bmatrix} 0 & 0 & 0 & 0 & 0 & 0 & 0 & 0 \\ 1 & 0 & 0 & 0 & 0 & 0 & 0 & 1 \\ 0 & 0 & 0 & 0 & 0 & 1 & 0 & 0 \\ 0 & 0 & 0 & 1 & 0 & 0 & 1 & 0 \\ 0 & 1 & 0 & 0 & 1 & 0 & 0 & 0 \\ 0 & 0 & 1 & 0 & 0 & 0 & 0 & 0 \end{bmatrix}. \tag{6}$$

The MF's output is calculated by

$$y_m^{L_m}(t) = IFFT\left\{FFT\left[r(t)\right]FFT\left[h_m^{L_m}(t)\right]\right\}, \tag{7}$$

where FFT is the fast Fourier transform, $IFFT$ is the inverse FFT, and $r(t)$ is the received FCCW. Practically, this filtering process can be performed using the overlap-add method for every MF length $L_m T_h/\kappa$ [23]. However, this filtering process is not suitable for certain sonar systems that must update the distance estimate at intervals of T_h/κ.

Any FHT t_m and any length L_m of MF $h_m^{L_m}(t)$ can be represented by the linear combination of time-shifted GC:

$$g_i(t) = p(t)e^{-j2\pi\kappa(f_c+(i-1)F)_h t}, \quad 1 \le i \le L_f, 0 \le t \le \frac{T_h}{\kappa}. \tag{8}$$

Similarly, $y_m^{L_m}(t)$ can be represented by GC outputs $x_i(t) = IFFT\left\{FFT\left[r(t)\right]FFT\left[g_i(t)\right]\right\}$. The overlap-add method for $x_i(t)$ is performed every T_h/κ, and a row vector $\mathbf{x}_i(u)$ is the output obtained for every T_h/κ as follows:

$$\mathbf{x}_i(u) = IFFT\left\{FFT\left[\mathbf{r}(u)\right]FFT\left[g_i(t)\right]\right\}, \tag{9}$$

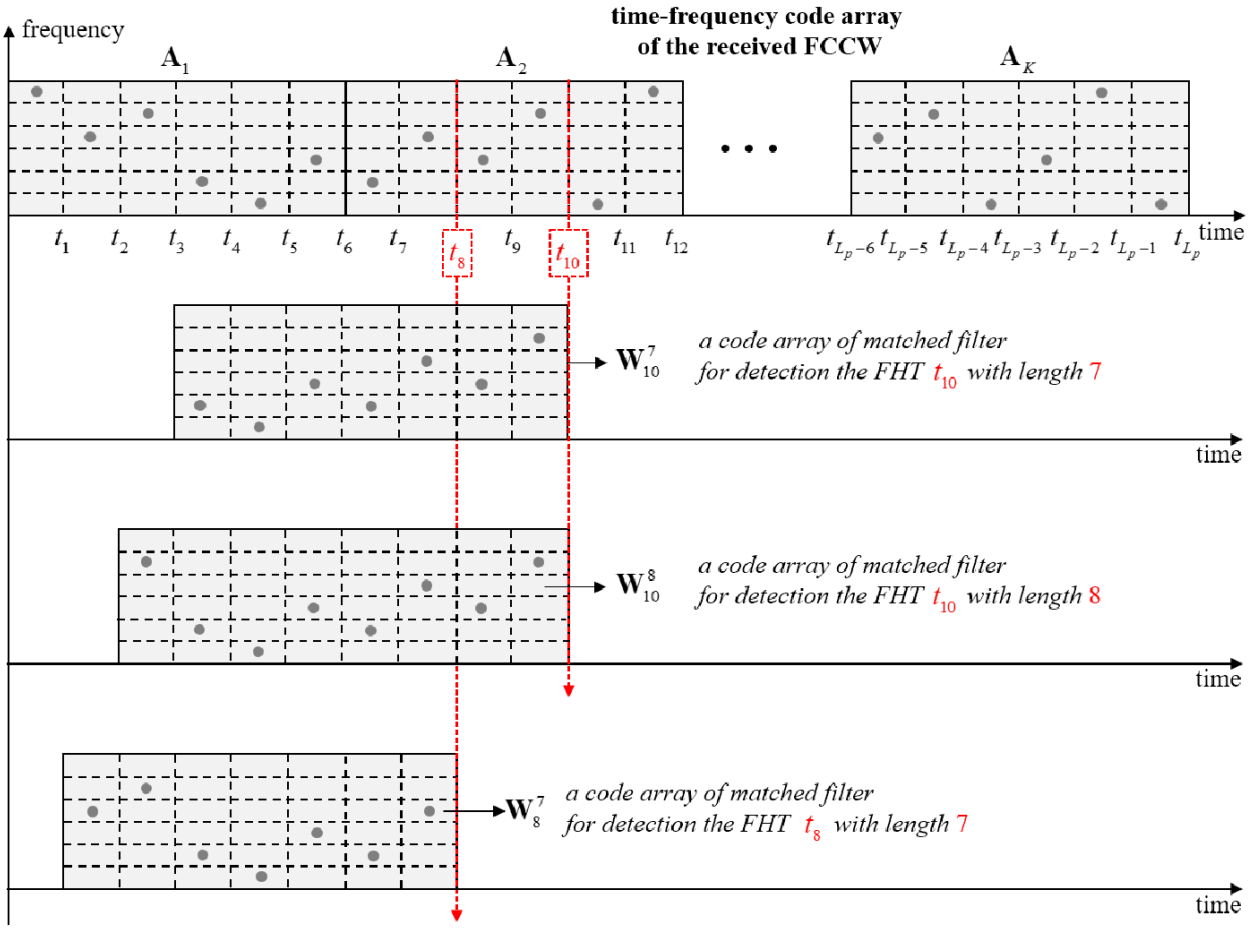

FIGURE 4. Examples of code arrays of matched filters for detection FHTs with several lengths.

where $\mathbf{r}(u)$ is u^{th} block data of a received FCCW to be calculated by the overlap-add method, as represented in Fig. 5. The calculation of $\mathbf{y}_m^{L_m}(u)$ using $\mathbf{W}_m^{L_m}$ and $\mathbf{x}_i(u)$ can be represented by

$$\begin{aligned}\mathbf{y}_m^{L_m}(u) &= \sum_{l=1}^{L_m}\sum_{i=1}^{L_f}\mathbf{W}_m^{L_m}(i,l)\,\mathbf{x}_i(u-l+1)\\ &= \sum_{l=1}^{L_m}\mathbf{z}_m^{L_m}(u-l+1)\,. \end{aligned} \tag{10}$$

The calculation examples of $\mathbf{y}_{10}^{8}(u)$, $\mathbf{y}_{11}^{8}(u+1)$, and $\mathbf{y}_{11}^{9}(u+1)$ are shown in Fig. 5. Many computations of $\mathbf{y}_{10}^{8}(u)$ and $\mathbf{y}_{11}^{8}(u+1)$ are shared as

$$\mathbf{y}_{10}^{8}(u) - \mathbf{z}_{10}^{8}(u-7) = \mathbf{z}_{10}^{8}(u-6) + \cdots + \mathbf{z}_{10}^{8}(u)\,, \tag{11}$$

$$\mathbf{y}_{11}^{8}(u+1) = \mathbf{y}_{10}^{8}(u) + \mathbf{z}_{11}^{8}(u+1) - \mathbf{z}_{10}^{8}(u-7)\,. \tag{12}$$

Similarly, many computations of $\mathbf{y}_{10}^{8}(u)$ and $\mathbf{y}_{11}^{9}(u+1)$ are also shared as

$$\mathbf{y}_{10}^{8}(u) = \mathbf{z}_{10}^{8}(u-7) + \mathbf{z}_{10}^{8}(u-6) + \cdots + \mathbf{z}_{10}^{8}(u)\,, \tag{13}$$

$$\mathbf{y}_{11}^{9}(u+1) = \mathbf{y}_{10}^{8}(u) + \mathbf{z}_{11}^{8}(u+1)\,. \tag{14}$$

The MF outputs $\mathbf{y}_m^{L_m}(u)$ based on the current block data $\mathbf{r}(u)$ are calculated by

$$\begin{aligned}\mathbf{y}_m^{L_m}(u) &= \mathbf{y}_{m-1}^{L_m}(u-1) + \mathbf{z}_m^{L_m}(u) - \mathbf{z}_{m-1}^{L_m}(u-L_m+1)\,,\\ &\qquad \textit{for } 2 \le m \le L_p,\\ \mathbf{y}_1^{L_m}(u) &= \mathbf{y}_{L_p}^{L_m}(u-1) + \mathbf{z}_1^{L_m}(u) - \mathbf{z}_{L_f}^{L_m}(u-L_m+1)\,. \end{aligned} \tag{15}$$

Equation (15) is the calculation corresponding to $h_m^{L_m}(t)$ with length $L_m T_h/\kappa$, which is generated by $\mathbf{W}_m^{L_m}$. If the MF's length is increased to $(L_m+1)\,T_h/\kappa$ in the current block, $\mathbf{y}_m^{L_m+1}(u)$ is calculated by

$$\begin{aligned}\mathbf{y}_m^{L_m+1}(u) &= \mathbf{y}_{m-1}^{L_m+1}(u-1) + \mathbf{z}_m^{L_m}(u)\,,\\ &\qquad \textit{for } 2 \le m \le L_p,\\ \mathbf{y}_1^{L_m+1}(u) &= \mathbf{y}_{L_p}^{L_m}(u-1) + \mathbf{z}_1^{L_m}(u)\,. \end{aligned} \tag{16}$$

The MF outputs $y_m^{L_m}(t)$ at all FHTs can be graphically viewed on a time-FHT map, as shown in Fig. 6. At the peaks of $y_m^{L_m}(t)$ and $y_{m+1}^{L_m}(t)$, there is a time difference of T_h/κ. By detecting the peaks of all $y_m^{L_m}(t)$, we can determine the target distance in the period T_h/κ. Details of detecting peaks and distance estimation will be explained in Sections 3.3 and 3.4.

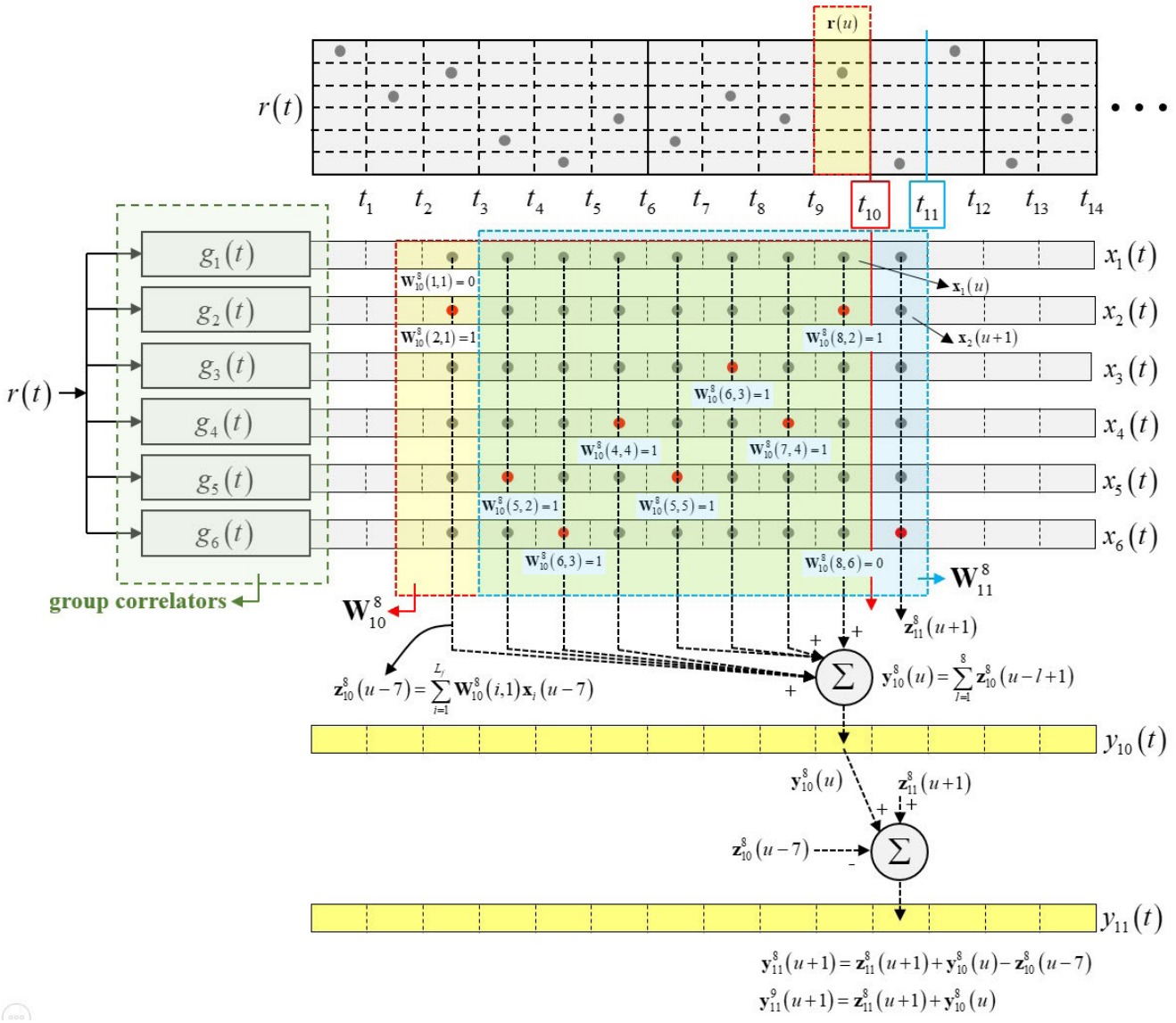

FIGURE 5. Basic concept of group correlators to implement all matched filter for FHTs detection.

The GC-based implementation of MFs for detecting the FHTs is considered to be meaningful in the following three aspects.

First, for the FCCW addressed in this study, FHTs must be detected, and distance estimates are obtained every T_h/κ interval. Therefore, the outputs of MFs for detecting all FHTs must be obtained every T_h/κ. If we implement the output for the $L_m T_h/\kappa$ length MF directly with the overlap-add method, L_m FHTs are detected after collecting signals for $L_m T_h/\kappa$ interval. Such an implementation may not be suitable for systems that must obtain distance estimates every T_h/κ interval, but GC-based matched filtering yields distance estimates every T_h/κ interval.

Second, L_f GC can implement all L_p MFs of various lengths with minimum computational complexity. The cost of complex multiplications of all L_p MFs implemented by the overlap-add method is nearly $O\left(L_p\,(L_m N_R)\log_2\,(L_m N_R)\right)$ for the block data $\mathbf{r}\,(u)\ \in\ \mathbb{R}^{1\times N_R}$ The cost of a GC-based overlap-add method is nearly $O\left(L_f N_R \log_2 N_R\right)$ because only L_f correlators for subpulses are used.

Last, GC-based implementation is suitable for filtering continuous-wave signals. In the filtering process of continuous waves, the acquisition time of the received signal can be extended to improve detection and estimation performance or to suppress reverberations.

B. ACCUMULATED SUM (AS) PROCESS

The AS process uses the MFs' output $\mathbf{y}_m^{L_m}\,(u)$ of multiple adjacent FHTs to detect a specific FHT and improves detection

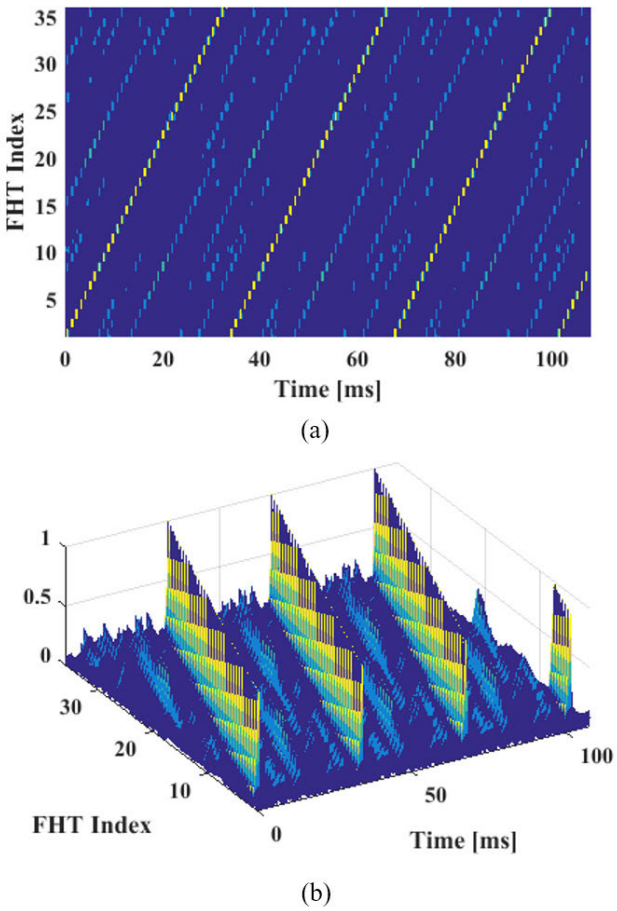

FIGURE 6. Example of the MF outputs of all FHTs; (a) top view, (b) side view.

and estimation performance in severe environments by accumulating peaks of adjacent $\mathbf{y}_m^{L_m}(u)$. An example of how to perform the AS process is shown in Fig. 7, and the output of the AS process $\mathbf{a}_m^{L_{as}}(u) \in \mathbb{R}^{1\times N_R}$ is defined by

$$\mathbf{a}_m^{L_{as}}(u) = \sum_{d=0}^{L_{as}-1} \left|\mathbf{y}_{m-d}^{L_m}(u-d)\right|,$$
$$\mathbf{a}_m^{L_{as}}(u) = \left[\mathbf{a}_m^{L_{as}}(u,1), \cdots, \mathbf{a}_m^{L_{as}}(u,v), \cdots, \mathbf{a}_m^{L_{as}}(u,N_R)\right], \tag{17}$$

where L_{as} is the number of blocks of $\mathbf{y}_m^{L_m}(u)$ accumulated, and v is the element index of a row vector $\mathbf{a}_m^{L_{as}}(u)$. In the $(u+1)^{th}$ block, the accumulated amount of the AS process can be adjusted as follows:

$$\mathbf{a}_m^{L_{as}}(u+1) = \mathbf{a}_{m-1}^{L_{as}}(u) + \mathbf{y}_m^{L_m}(u+1) - \mathbf{y}_{m-L_{as}+1}^{L_m}(u-L_{as}+1), \tag{18}$$

$$\mathbf{a}_m^{L_{as}+1}(u+1) = \mathbf{a}_{m-1}^{L_{as}}(u) + \mathbf{y}_m^{L_m}(u+1). \tag{19}$$

Fig. 8 shows an example of time-FHT maps (TFM) for $\mathbf{y}_m^{L_m}(u)$ and $\mathbf{a}_m^{L_{as}}(u)$ in a noisy environment (SNR $= -33$ dB). In case $\mathbf{a}_m^{L_{as}}(u)$, as shown in Fig. 8-(b), $L_{as} = 50$ blocks are accumulated.

C. TIME-DELAY MAP FOR DISTANCE ESTIMATION

The detection process for the FHTs is performed on the AS output data of each block unit as follows:

$$\Lambda^{L_{as}}(u) = \begin{bmatrix} \mathbf{a}_1^{L_{as}}(u) \\ \vdots \\ \mathbf{a}_m^{L_{as}}(u) \\ \vdots \\ \mathbf{a}_{L_p}^{L_{as}}(u) \end{bmatrix} \in \mathbb{R}^{L_p\times N_R}, \tag{20}$$

$$\Lambda_{\max}^{L_{as}}(u) = \begin{bmatrix} \mathbf{a}_1^{L_{as}}(u, v_{\max-1}) \\ \vdots \\ \mathbf{a}_m^{L_{as}}(u, v_{\max-m}) \\ \vdots \\ \mathbf{a}_{L_p}^{L_{as}}(u, v_{\max-L_p}) \end{bmatrix} \in \mathbb{R}^{L_p\times 1}, \tag{21}$$

where $\mathbf{a}_m^{L_{as}}(u, v_{\max-m})$ is the maximum value of the row vector $\mathbf{a}_m^{L_{as}}(u)$, and $v_{\max-m}$ becomes a specific sample index for $\mathbf{a}_m^{L_{as}}(u)$. Among the elements of $\Lambda_{\max}^{L_{as}}(u)$, the upper N_{Up} of larger values are used for distance estimation. $\Lambda_{desc}^{L_{as}}(u)$ is $\Lambda_{\max}^{L_{as}}(u)$ sorted in descending order, and q is the element index for $\Lambda_{desc}^{L_{as}}(u)$, where $\boldsymbol{\eta}(q)$ is an FHT index corresponding to q^{th} element of $\Lambda_{desc}^{L_{as}}(u)$.

To robustly estimate a target's distance, we define time-FHT lines and derive a time-delay map (TDM). In Fig. 9, there is a transmitter's FHT line $\boldsymbol{\psi}_T(n)$ and an AS output's FHT line $\boldsymbol{\psi}_q(u)$ corresponding to $\mathbf{a}_m^{L_{as}}(u, v_{\max-m})$, which are defined as follows:

$$\boldsymbol{\psi}_T(u) = \begin{bmatrix} n \\ \psi_T[n] = \bmod\left(n, L_pN_T\right) \end{bmatrix}, \tag{22}$$

$$\boldsymbol{\psi}_q(u) = \begin{bmatrix} n_q \\ \psi_q[n_q] = (\boldsymbol{\eta}(q)-1)L_p \end{bmatrix}, \tag{23}$$

$$n_q = (u-1)N_R + v_{\max-\boldsymbol{\eta}(q)}, \tag{24}$$

where n is a sample index; N_T and N_R are sample numbers of subpulses in transmitted and received FCCW; and n_u is a sample index for $\mathbf{a}_{\boldsymbol{\eta}(q)}^{L_{as}}\left(u, v_{\max-\boldsymbol{\eta}(q)}\right)$.

The TDM is drawn using $\boldsymbol{\psi}_T(u)$ and multiple $\boldsymbol{\psi}_q(u)$, as given by

$$\zeta_q(u) = \begin{bmatrix} n_q \\ \zeta_q[n_q] \end{bmatrix},$$
$$\zeta_q[n_q] = \bmod\left[\psi_T[n_q] - \psi_q[n_q] + L_pN_T, L_pN_T\right]. \tag{25}$$

If the target's Doppler ratio is constant with κ, $\zeta_q(u)$ will be drawn as a line with a slope of $1-\kappa$, as shown in Fig. 10.

D. DOPPLER LINE FITTING FOR MULTIPLE TARGETS

The classification of multiple targets is performed only for the line $\zeta_q(u)$ with the slope of $1-\kappa$ in the TDM. We use a least-square fit method to determine whether sequential data of $\zeta_q(u)$ has a slope of $1-\kappa$ as follows:

$$E_q(u) = \sqrt{\frac{1}{K_l}\sum_{k=0}^{K_l-1}\left(\mathbf{W}_{line}^T\mathbf{X}_q(u-k)\right)^2} < \varepsilon, \tag{26}$$

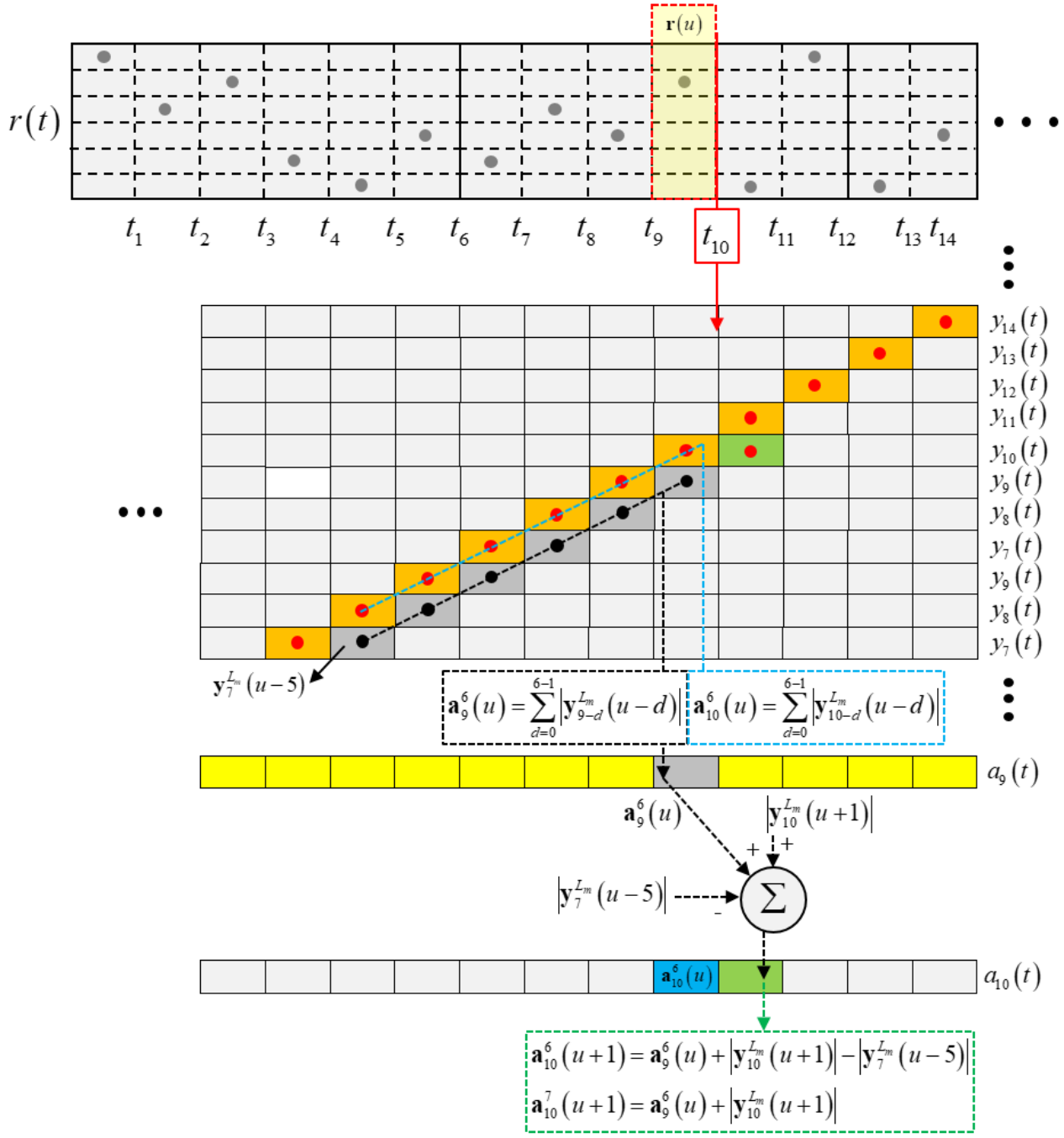

FIGURE 7. Basic concept of the AS process.

$$\mathbf{W}_{line} = [\kappa - 1,\ 1,\ \tau_0]^T, \tag{27}$$

$$\mathbf{X}_q(u) = \left[\zeta_q(u)^T,\ 1\right]^T, \tag{28}$$

where K_l is the number of blocks, and τ_0 is an initial delay time. If there is a fitting error $E_m(u)$ less than ε for any τ_0, a target exits, and $\zeta_q(u)$ becomes a distance estimate of the corresponding target.

Fig. 11 shows the TDM of $N_{Up} = 1, 2, 3$ for two targets, and $\zeta_q(u)$ for the upper $N_{Up} = 2$ of larger values of $\Lambda_{\max}^{L_{as}}(u)$ forms blue and red lines with the slope of $1 - \kappa$ in TDM. The method presented in this paper is a basic approach for detecting targets using curve fitting in TDM and can be designed using advanced techniques.

E. COMPARISON OF THE PROPOSED METHOD AND SLO-CO

Although GCAS was performed independently of SLO-CO [20], similarities and differences that are related to the Doppler effect, acquisition time, and practical implementations exist. The GCAS shown as a modified version of

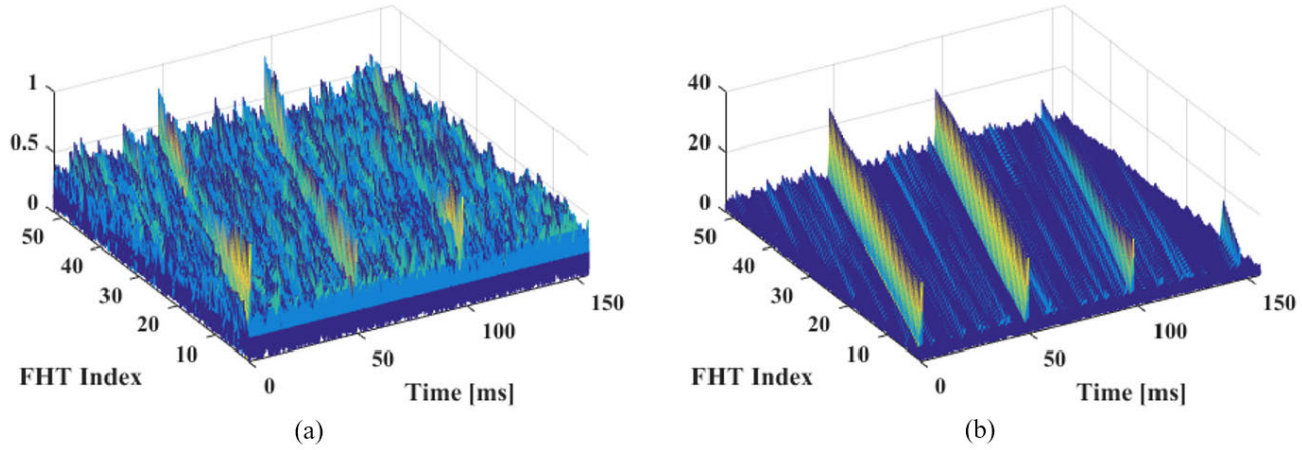

FIGURE 8. Example of the time-FHT map (TFM); (a) GC output, (b) AS output.

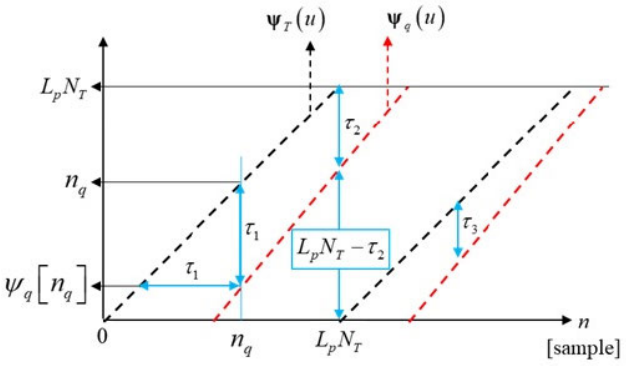

FIGURE 9. Basic concept of FHT lines of transmitted FCCW and AS output.

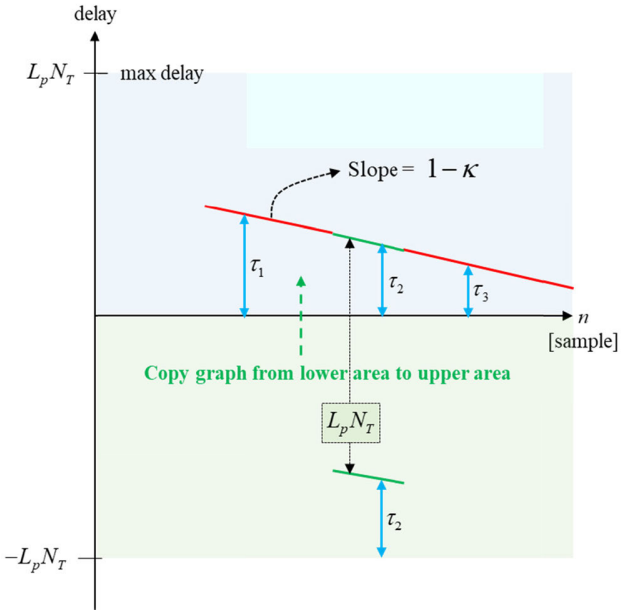

FIGURE 10. Time-delay map corresponding to Fig. 9.

SLO-CO is used in an LPI underwater seeker. The similarities and distinctions between the GCAS and SLO-CO are as follows:

Similarities: (1) L_p (= 77) MFs are used to detect all L_p (= 77) FHTs, as shown in Fig. 12-(a).

(2) MF outputs are accumulated to obtain reliable detection results of FHTs, as shown in Fig. 12-(b).

Distinctions: (1) We consider extremely high Doppler environments, but SLO-CO does not. The shrinkage of signal length is not reflected on the MF output of SLO-CO, as shown in Fig. 13. While Doppler frequency and bandwidth expansion are exactly reflected on the MF of SLO-CO, the length of MF, L_fT_h (= $11 \times 1ms$), is fixed by the length of the transmitted signal; this makes it convenient to implement Doppler correlators. However, SLO-CO cannot obtain reliable outputs of MFs because a large correlation loss occurs between received FCCW and MFs, as shown in Fig. 13-(b).

(2) In the SLO-CO processing algorithm, it is assumed that distance estimates obtained from different FHTs in a repetition interval are nearly identical due to the low speed of a target. Additionally, multiple detection results for FHTs are combined as a distance estimate in a repetition interval L_pT_h. However, GCAS deals with cases where distance estimates obtained from multiple FHTs in a repetition interval $L_pT_h = 77ms$ are progressively decreased (or increased), as shown in Fig. 14, because the speeds of an underwater seeker and a target are so fast that the Doppler effect cannot be approximated using the Doppler shift model. However, AS processing combines the multiple detection results of adjacent FHTs to obtain reliable detection results of all FHTs, and distance estimates are updated for every FHT. Fig. 15-(a) shows the detected FHT index of only GC and GC+ AS every $T_h/\kappa \approx 0.936ms$. Thus, AS processing is required to increase the acquisition time to obtain the correct index of FHTs in low SNR environments because the false FHT index causes large distance errors, as shown in Fig. 15-(b).

(3) The SLO-CO processing algorithm does not include the practical implementation of multiple matched filtering [21]. Multiple matched filtering is implemented with a convolution operation, which is inappropriate in many MFs and Doppler correlators with high sampling frequency.

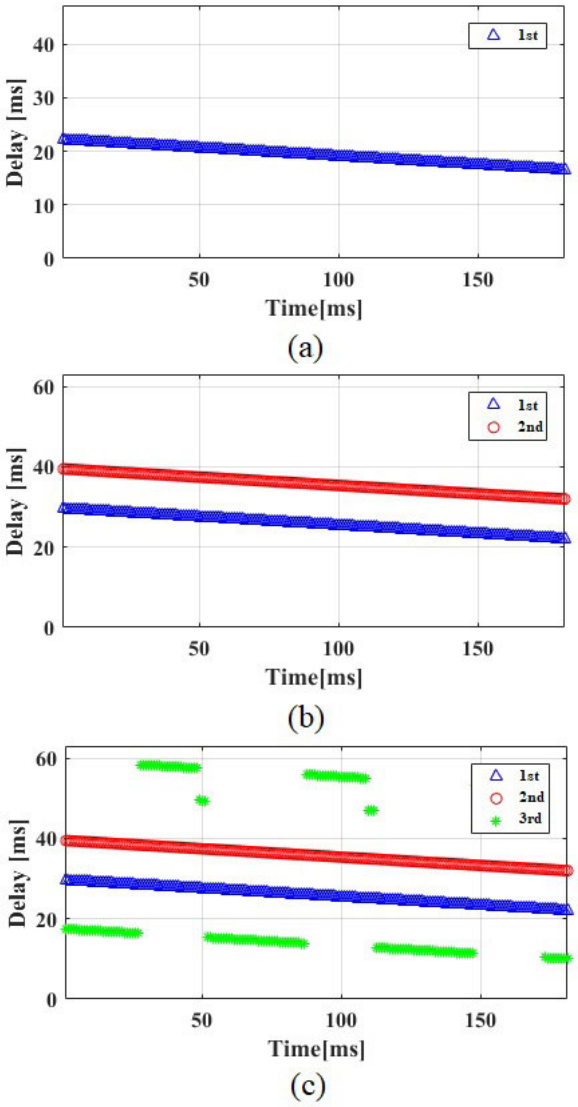

FIGURE 11. Example of TDM with two targets; (a) $N_{Up} = 1$, (b) $N_{Up} = 2$, (c) $N_{Up} = 3$.

Conversely, in GCAS, L_p MFs with the length of $L_m T_h/\kappa$ can be implemented by only L_f subpulse correlators ($L_f \ll L_p$) with the length of T_h/κ. Even if the number of MFs L_p and the number of subpulses L_m increase, only complex addition is required with few complex multiplications.

IV. SIMULATION RESULTS

To investigate using FCCW and the purpose of GCAS, we performed simulations in severe environments with a large Doppler effects and low SNR. The simulation parameters used are shown in Table 1. Considering that target movement can be directly transformed into a delay and Doppler ratio, we represent target movement as the delay and Doppler frequency measurements. We primarily referred to SLO-CO [20] to determine the parameters of the proposed simulations. The proposed detection and estimation methods for the

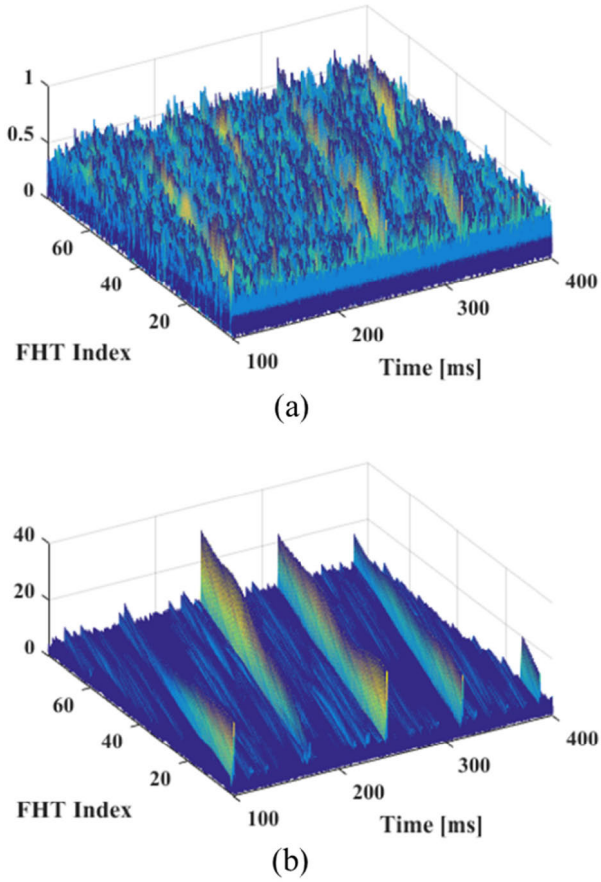

FIGURE 12. Comparison of the time-FHT maps, SNR = −30 dB; (a) GC output, (b) AS output with $L_{as} = 50$.

TABLE 1. Simulation parameters.

Parameters	Variable and Values
Carrier frequency	f_c
Sampling frequency	$f_s = 10 f_c$
Hopping-frequency	$f_h = 1\text{kHz}$
Hopping-interval	$T_h = 1\text{ms} \rightarrow N_T = 1000$
# of frequency state	$L_f = 7$
# of subarray	$K = 11$
# of total subpulse	$L_p = 77 \rightarrow PRI = 77\text{ms}$
SNR	-28, -30, -32 dB
Doppler ratio	$\kappa = 1.0026$ (relative speed = 2 m/s) $\kappa = 1.0689$ (relative speed = 50 m/s)
MF length	$L_m = 20$ $(\rightarrow T_h L_m/\kappa \approx 18.71\text{ms})$
AS length	$L_{as} = 10, 20, 30, 40, 50$
# of trials	100

FCCW can increase the acquisition time to reliably detect FHTs and to accurately estimate the target distance in low SNR environments, which is the AS process. The detection probabilities (PDs) for FHTs increase as lengths increase,

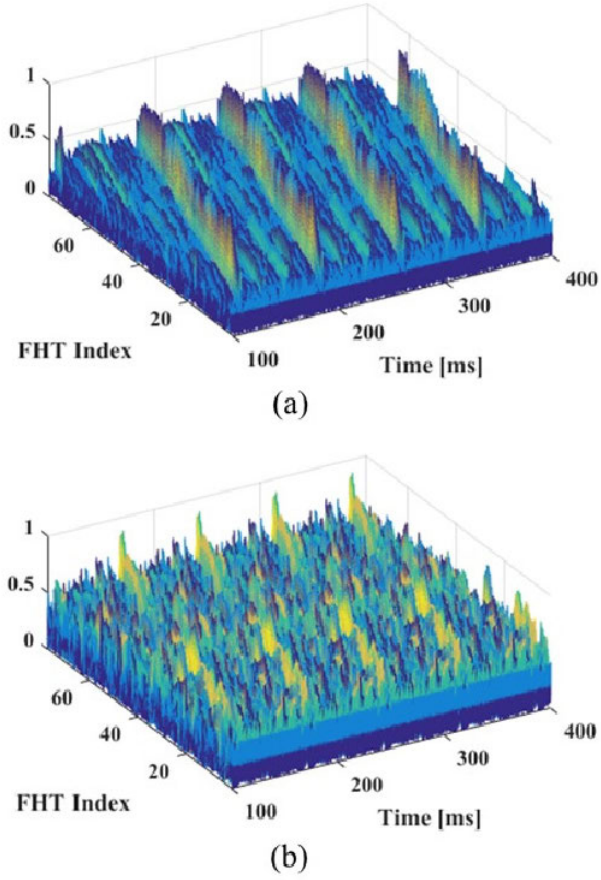

FIGURE 13. Time-FHT maps for MF outputs of SLO-CO; (a) $\kappa = 1.0026$, (b) $\kappa = 1.0689$.

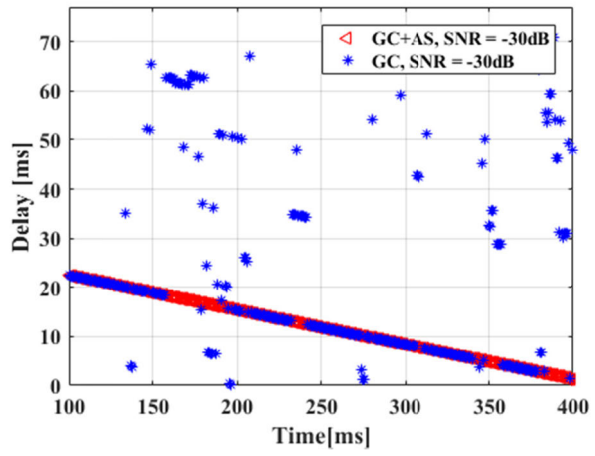

FIGURE 14. TDM in the case of SNR $= -30$ dB and $L_{as} = 50$.

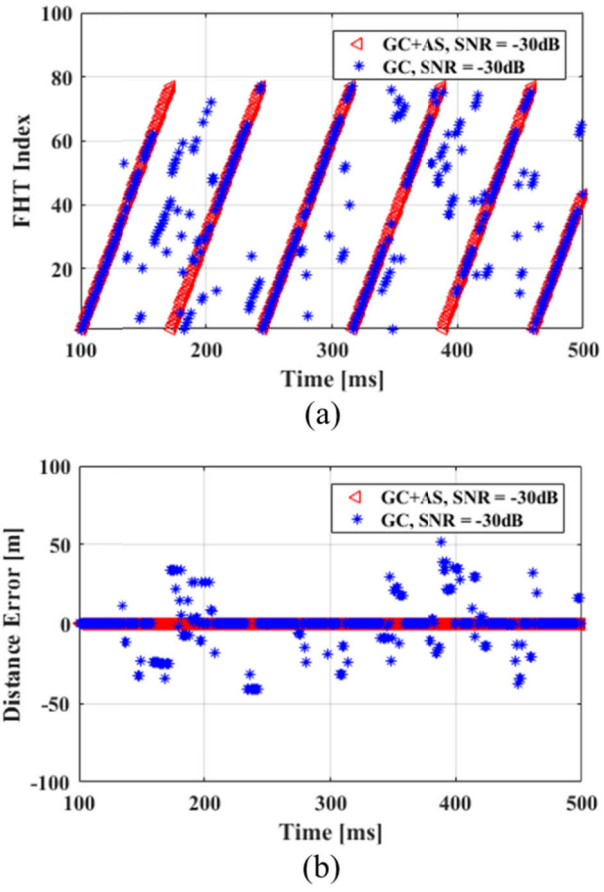

FIGURE 15. Detected FHTs and distance error, SNR $= -30$ dB; (a) detected FHTs, (b) distance error.

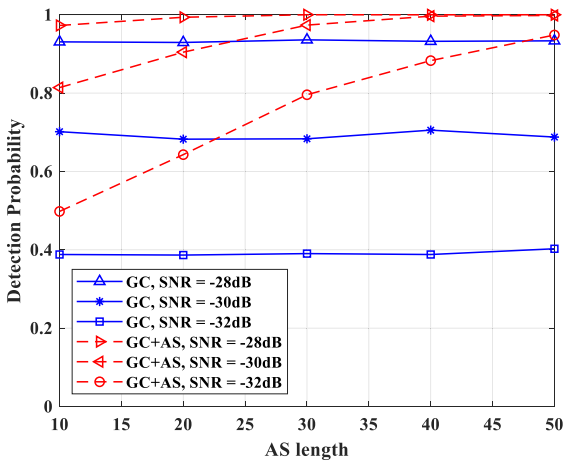

FIGURE 16. Detection probabilities based on SNRs and AS length.

as shown in Fig. 15. With an SNR of -28 and -30 dB, PDs are near one with AS length of $L_{as} = 40$, where the acquisition time is $(L_m + L_{as})T_h/\kappa \approx 56.1324$. The root-mean-square errors (RMSEs) of distance estimate of Fig. 16 are shown in Fig. 17. False detections of FHTs are shown to yield large distance errors in Fig. 15. Similarly, the RMSEs in Fig. 17 are sufficiently small when PDs approach one, as shown in Fig. 16. Based on these simulations, a sufficient acquisition time must be secured to reliably detect FHTs, or a robust procedure of distance estimation is required to overcome the false detection of FHTs.

Reverberation: We also performed simulations of the proposed distance estimation method in a reverberation environment. Because this paper considers continuous waves, this

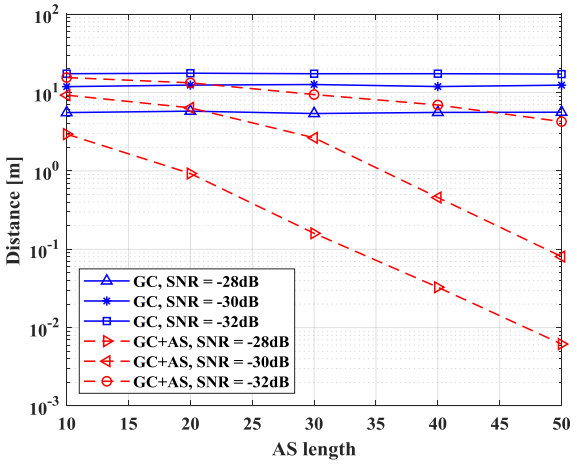

FIGURE 17. Distance RMSEs based on SNRs and AS length.

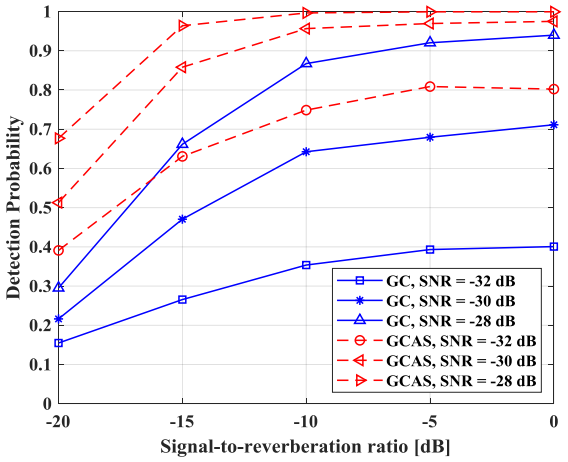

FIGURE 18. Detection probabilities based on SRRs and SNRs.

signal is significantly affected by volume reverberation [28]; thus, we simulated volume reverberation signals.

Volume reverberation waves can be produced by a linear filter model [29]. This reverberation model is based on two assumptions. First, the scatter density in the unit volume is sufficiently high and uniformly distributed. Second, this model assumes that only the first reflection occurs. From these assumptions, the reverberant channel with the scattering coefficient is described by

$$h_r(n) = \beta\alpha(n)\omega_r(n), \tag{29}$$

$$\alpha(n) = -20\log(0.5cT_sn), \tag{30}$$

where $\alpha(n)$ is a damping factor, β is a scaling factor with respect to the reverberation power, T_s is the sampling period, and $\omega_r(n)$ denotes nonscaled coefficients. The volume reverberation $w(n)$ is obtained from the convolution product of $h_r(n)$ and the transmitted wave $x(n)$ via:

$$w(n) = \sum_{k=1}^{N} x(n)h_r(k-n), \tag{31}$$

where N denotes the total number of samples.

To demonstrate the proposed method's reliability in a volume-reverberation environment, we conducted the same simulations except with reverberation. Figs. 18 and 19 show the detection probabilities and the RMSEs to the signal-to-reverberation ratio (SRR). In these cases, the AS length is set to 30. Volume reverberation is shown to degrade the performance of both the GCAS- and GC-based distance estimators. However, the RMSE of the GCAS is much lower than the GC-based method, as shown in Fig. 18. In particular, the GCAS can estimate target distance with an error of meters even when the SNR is -28 dB, and the SRR is -15 dB. Similarly, the detection performance in Fig. 19 also shows that the GCAS outperforms the GC-based method.

Fig. 20 also shows the RMSEs and the detection probabilities to the SRRs and the AS length. In this figure, we set the SNR as -30 dB. As an MF, a longer AS length yields improved processing gain and overcomes the reverberation

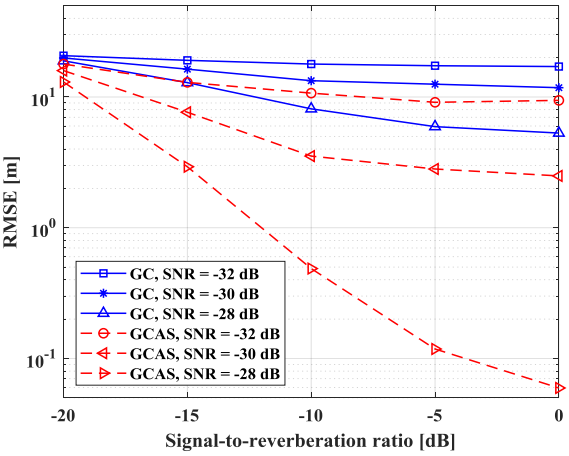

FIGURE 19. Distance RMSEs based on SRRs and SNRs.

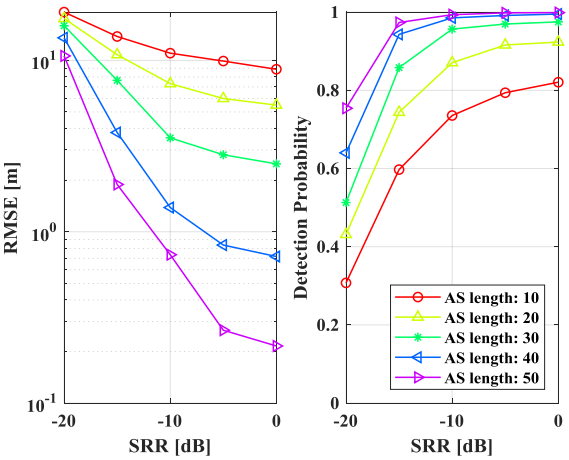

FIGURE 20. RMSE (left) and detection probability (right) of GCAS based on SRRs and AS length (SNR = −30 dB).

environment, highlighting the importance of signal length control.

V. CONCLUSION

In this paper, a near-range CAS scheme is proposed to estimate the distance of high-speed underwater targets, and FCCW is applied in the proposed CAS scheme to continuously estimate a target distance and to obtain LPI characteristics. Sonar systems that describe LPI characteristics may have low SNR due to their low transmission powers. The proposed CAS scheme can obtain reliable distance estimates by increasing the acquisition time for CW with a fixed calculation amount. In the future, we plan to study how to determine a sufficient acquisition time for a specific SNR environment and to eliminate false FHT detections in the distance estimation process.

REFERENCES

[1] G. R. Mellema, "Improved active sonar tracking in clutter using integrated feature data," *IEEE J. Ocean. Eng.*, vol. 45, no. 1, pp. 304–318, Jan. 2020.

[2] S. Yao, W. Yu, S. Fang, and S. Huang, "Robust active sonar detection in frequency and time dispersive channels using matching envelope spectrum of multi-pulse LFM signals," *IEEE Access*, vol. 8, pp. 159990–160003, Aug. 2020.

[3] G. Delyon, "Clutter map detector for active diver detection sonar," *IET Radar, Sonar Navigat.*, vol. 14, no. 1, pp. 177–186, Jan. 2020.

[4] R. V. Vossen, S. P. Beerens, and E. V. D. Spek, "Anti-submarine warfare with continuously active sonar—TNO tests the principles of continuously active sonar with the interim removable low-frequency active sonar system," *Sea Technol.*, vol. 52, no. 11, pp. 33–35, Nov. 2011.

[5] P. C. Hines, "Experimental comparison of continuous active and pulsed active sonars in littoral waters," in *Proc. 1st Int. Conf. Exhib. Underwater Acoust.*, vol. 7, May 2013, pp. 51–58.

[6] A. Munafo, G. Canepa, and K. D. LePage, "Continuous active sonars for littoral undersea surveillance," *IEEE J. Ocean. Eng.*, vol. 44, no. 4, pp. 1198–1212, Oct. 2019.

[7] G. Canepa, A. Munafo, M. Micheli, L. Morlando, and S. Murphy, "Real-time continuous active sonar processing," in *Proc. OCEANS*, Genoa, Italy, May 2015, pp. 1–6.

[8] S. M. Murphy, P. C. Hines, and K. Dunphy, "Classifying continuous active sonar echoes for target recognition," in *Proc. Int. Conf. Exhib. Underwater Acoust.*, May 2014, pp. 811–818.

[9] Y. Wang and J. Yang, "Continuous transmission frequency modulation detection under variable sonar-target speed conditions," *Sensors*, vol. 13, no. 3, pp. 3549–3567, Mar. 2013.

[10] R. B. Wynn, V. A. I. Huvenne, T. P. Le Bas, B. J. Murton, D. P. Connelly, B. J. Bett, H. A. Ruhl, K. J. Morris, J. Peakall, D. R. Parsons, E. J. Sumner, S. E. Darby, R. M. Dorrell, and J. E. Hunt, "Autonomous underwater vehicles (AUVs): Their past, present and future contributions to the advancement of marine geoscience," *Mar. Geol.*, vol. 352, pp. 451–468, Jun. 2014.

[11] H. K. Heidarsson and G. S. Sukhatme, "Obstacle detection and avoidance for an autonomous surface vehicle using a profiling sonar," in *Proc. IEEE Int. Conf. Robot. Automat.*, Shanghai, China, May 2011, pp. 731–736.

[12] L. Paull, S. Saeedi, M. Seto, and H. Li, "AUV navigation and localization: A review," *IEEE J. Ocean. Eng.*, vol. 39, no. 1, pp. 131–149, Jan. 2014.

[13] H.-H. Ko, K.-W. Cheng, and H.-J. Su, "Range resolution improvement of FMCW radars," in *Proc. 5th Eur. Radar Conf.*, Amsterdam, The Netherlands, Oct. 2008, pp. 352–355.

[14] M. Kunita, M. Sudo, and T. Mochizuki, "Range measurement in ultrasound FMCW signals," in *Proc. IEEE Ultrason. Symp.*, Beijing, China, Nov. 2008, pp. 1366–1369.

[15] A. Y. Erdogan, T. O. Gulum, L. Durak-Ata, T. Yildirim, and P. E. Pace, "FMCW signal detection and parameter extraction by cross Wigner-Hough transform," *IEEE Trans. Aerosp. Electron. Syst.*, vol. 53, no. 1, pp. 334–344, Feb. 2017.

[16] A. Anghel, G. Vasile, R. Cacoveanu, C. Ioana, and S. Ciochina, "Short-range wideband FMCW radar for millimetric displacement measurements," *IEEE Trans. Geosci. Remote Sens.*, vol. 52, no. 9, pp. 5633–5642, Sep. 2014.

[17] S. P. Pecknold, W. M. Renaud, D. R. McGaughey, J. A. Theriault, and R. F. Marsden, "Improved active sonar performance using costas waveforms," *IEEE J. Ocean. Eng.*, vol. 34, no. 4, pp. 559–574, Oct. 2009.

[18] S. M. Murphy and P. C. Hines, "Sub-band processing of continuous active sonar signals in shallow water," in *Proc. OCEANS*, Genoa, Italy, May 2015, pp. 1–4.

[19] H. DeFerrari and J. Wylie, "Ideal signals and processing for continuous active sonar," in *Proc. Meetings Acoust.*, vol. 19, Feb. 2013, Art. no. 055058.

[20] G. Hickman and J. L. Krolik, "Non-recurrent wideband continuous active sonar," in *Proc. Oceans*, Hampton Roads, VA, USA, 2012, pp. 1–6.

[21] Y.-K. Seo, W.-J. Kim, and H.-N. Kim, "Range estimation method in a short-range FMCW SONAR," in *Proc. 36th IASTED Int. Conf. Modelling, Identificat. Control*, Innsbruck, Austria, Jan. 2017, pp. 251–254.

[22] Y.-K. Seo, D.-G. Kim, W.-S. Son, and H.-N. Kim, "Design of a hopping-frequency coding based transmission method for underwater detection," in *Proc. Int. Conf. Electron., Inf., Commun. (ICEIC)*, Honolulu, HI, USA, Jan. 2018, pp. 878–881.

[23] Y.-K. Seo, W.-S. Son, H.-N. Kim, and W.-J. Kim, "Distance estimation for hopping frequency coding based continuous wave," in *Proc. Int. Conf. Green Hum. Inf. Technol. (ICGHIT)*, Chiang Mai, Thailand, Feb. 2018, pp. 268–271.

[24] P. E. Pace, *Detecting and Classifying Low Probability of Intercept Radar*. Norwood, MA, USA: Artech House, 2008.

[25] A. De Maio, S. De Nicola, Y. Huang, Z.-Q. Luo, and S. Zhang, "Design of phase codes for radar performance optimization with a similarity constraint," *IEEE Trans. Signal Process.*, vol. 57, no. 2, pp. 610–621, Feb. 2009.

[26] J. J. Benedetto, I. Konstantinidis, and M. Rangaswamy, "Phase-coded waveforms and their design," *IEEE Signal Process. Mag.*, vol. 26, no. 1, pp. 22–31, Jan. 2009.

[27] N. Touati, C. Tatkeu, T. Chonavel, and A. Rivenq, "Phase coded costas signals for ambiguity function improvement and grating lobes suppression," in *Proc. IEEE 78th Veh. Technol. Conf. (VTC Fall)*, Sep. 2013, pp. 1–5.

[28] Q. Li, *Digital Sonar Design in Underwater Acoustics, Advanced Topics in Science and Technology in China*. Berlin, Germany: Springer, 2012. [Online]. Available: https://link.springer.com/book/10.1007/978-3-642-18290-7#about

[29] Y. Seo, G.-H. Park, W.-J. Kim, and H.-N. Kim, "Distance estimation for hopping-frequency-coding-based continuous wave," *J. Intell. Fuzzy Syst.*, vol. 35, no. 6, pp. 6181–6188, Dec. 2018.

GEUN-HO PARK received the B.S., M.S., and Ph.D. degrees in electronic and electrical engineering from Pusan National University, Busan, South Korea, in 2013, 2015, and 2020, respectively. Since March 2020, he has been a Researcher with the Department of Electrical and Computer Engineering, Pusan National University. Since December 2020, he has been a Researcher with the Defense Agency for Technology and Quality, South Korea. His research interests include digital signal processing, array signal processing, radar signal processing, electronic warfare systems, and machine learning.

YOUNG-KWANG SEO received the B.S., M.S., and Ph.D. degrees in electronic and electrical engineering from Pusan National University, Busan, South Korea, in 2012, 2014, and 2019, respectively. From 2019 to 2020, he was a Researcher with the Department of Electrical and Computer Engineering, Pusan National University. Since March 2020, he has been a Senior Researcher with Hanwha Systems, South Korea. His research interests include radar signal processing, sonar signal processing, and machine learning (ML).

WAN-JIN KIM received the B.S., M.S., and Ph.D. degrees in electronic and electrical engineering from Pusan National University (PNU), Busan, South Korea, in 2005, 2007, and 2011, respectively. He is currently working with the Agency for Defense Development, South Korea. His research interests include digital signal processing, OFDM systems, adaptive filtering, radar/sonar signal processing, signal processing for digital broadcasting, and digital communications.

HYOUNG-NAM KIM (Member, IEEE) received the B.S., M.S., and Ph.D. degrees in electronic and electrical engineering from the Pohang University of Science and Technology, Pohang, South Korea, in 1993, 1995, and 2000, respectively. From 2000 to 2003, he was with the Electronics and Telecommunications Research Institute, Daejeon, South Korea, developing advanced transmission and reception technology for terrestrial digital television. In 2003, he joined the Department of Electronics Engineering, Pusan National University, Busan, South Korea, as a Faculty Member, where he is currently a full-time Professor. From 2009 to 2010, he was a Visiting Scholar with the Department of Biomedical Engineering, Johns Hopkins University School of Medicine. From 2015 to 2016, he was a Visiting Professor with the School of Electronics and Computer Engineering, University of Southampton, U.K. His research interests include digital signal processing, radar/sonar signal processing, adaptive filtering, and biomedical signal processing, digital communications, electronic warfare support systems, and brain–computer interface. He is also a member of IEIE and KICS.